Wave field in two-phase media by the convolutional differentiator method[*]

Zhuo Ye[1,3]   Xinfu Li[2]   and   Qiusheng Li[1,3,♣]

[1] *Institute of Geology, Chinese Academy of Geological Sciences, Beijing 100037, China*
[2] *School of Geophysics and Information Technology, China University of Geosciences,*
Beijing 100083, China
[3] *Earthprobe and Geodynamics Open Laboratory of Chinese Academy of Geological Sciences,*
Beijing 100037, China

Abstract   This paper applies the convolutional differentiator method, based on generalized Forsyte orthogonal polynomial (CFPD), to simulate the seismic wave propagation in two-phase media. From the numerical results we can see that three types of waves, fast P-waves, S-waves and slow P-waves, can be observed in the seismic wave field. The experiments on anisotropic models demonstrate that the wavefront is elliptic instead of circular and S-wave splitting occurs in anisotropic two-phase media. The research has confirmed that the rules of elastic wave propagation in fluid-saturated porous media are controlled by Biot's theory. Experiment on a layered fault model shows the wavefield generated by the interface and the fault very well, indicating the effectiveness of CFPD method on the wavefield modeling for real layered media in the Earth. This research has potential applications to the investigation of Earth's deep structure and oil/gas exploration.

Key words: convolutional Forsyte polynomial differentiator (CFPD); two-phase media; seismic wave field; numerical modeling
CLC number: P315.3$^+$1   **Document code**: A

1 Introduction

According to the elastic theory for two-phase media, the media in the Earth's interior is composed of solid phase that is porous and homogeneously isotropic and fluid phase that is viscous and saturated. The two-phase media can represent real materials to some extent and the relevant theories have been vastly developed and have improved seismic exploration significantly. Gassmann (1951) proposed the elastic wave propagation theory in porous elastic solids and established the famous Gassmann's equations that describe quantitatively the relationship between seismic velocity and porosity of the media. Then Biot (1956a, b) improved Gassmann's theory and laid the foundation of the theory for two-phase media.

Biot's equations for the propagation of elastic wave in fluid-saturated porous media stimulate the elastic wave propagation in two-phase media (Biot, 1956a, b). Wave equations established by Biot can be easily handled in the situation of homogeneous media, however, it is impossible to obtain the analytical solutions in the presence of arbitrary heterogeneities in the media. Numerous numerical simulation methods have been developed by seismologists to solve this problem. The widely used methods include finite difference method (FDM), finite element method and the Fourier method as well as the spectral-element method, each of which has its own merits and drawbacks (Zhou and Greenhalgh, 1992).

Seismologists all over the world have done a lot of amazing works to promote the development of the numerical modeling method in two-phase media. Zhu and McMechan (1991) simulated the wave field in two-phase media with finite difference method; Niu et al. (1994) discussed the wave equation and the its solution with finite element method for cracked anisotropic media saturated by fluid and gas; Dai et al. (1995) sim-

ulated the wave field in anisotropic two-phase media by solving the first-order velocity-stress wave equation; the computational formulas of the wave equation for the fluid-saturated porous media with a artificial boundary were derived by Shao and Lan (2000) based on finite element method; Yang (2002) simulated the elastic wave propagation in two-phase periodic thin layers (PTL) media and isotropic two-phase media with finite element method; the pseudo-spectral numerical resolution and finite element resolution for wave propagation in anisotropic two-phase media were obtained by Liu and Li (2000) and Liu and Wei (2003); Sun and Yang (2004) resolved the problems of frequency dispersion and stability by adopting the staggered-grid technique; the arbitrary even-order finite difference resolution of the velocity-stress wave equation for three-dimensional anisotropic two-phase media was given by Pei (2006).

In this paper, a convolutional differentiator method based on generalized Forsyte orthogonal polynomial, which was developed by Cheng et al. (2008) and applied to model seismic wave propagation in heterogeneous media by Li and Li (2008), is applied to the numerical simulation of seismic wave propagation in heterogeneous two-phase media. It has been proved that the method has the advantages of both high computation efficiency

and precision. Here, the spatial derivatives of the wave equations are computed by convolutional Forsyte polynomial differentiator and the temporal derivatives are computed by first-order staggered-grid finite-difference scheme. The results demonstrate that the method is reliable and competent for seismic wave modeling in real media.

2 Splitting of the first-order velocity-stress equations

Biot's theory for the elastic wave propagation in a fluid-saturated porous media describes the characteristics of wave field in fluid-saturated porous solid. Biot's theory is based on the following assumptions: (1) the fluid phase is continuous and the pores are connected; (2) the porous materials are statistically isotropic; (3) the size of the seismic wavelength is much larger than that of the pores; (4) the deformations of the solid framework are small; (5) the solid matrix is elastic; (6) there is no relative displacement occurs between the fluid and solid phase; (7) the dispersion and gravity are negligible.

The first-order velocity-stress can be written as follows:

1) Velocity component of the fluid phase

$$
\left(\rho_{12}^2 - \rho_{11}\rho_{22}\right)
\begin{bmatrix} \dfrac{\partial V_x}{\partial t} \\[2mm] \dfrac{\partial V_y}{\partial t} \\[2mm] \dfrac{\partial V_z}{\partial t} \end{bmatrix}
= \rho_{12}
\begin{bmatrix} \dfrac{\partial \sigma_{xx}}{\partial x} + \dfrac{\partial \tau_{xy}}{\partial y} + \dfrac{\partial \tau_{xz}}{\partial z} \\[2mm] \dfrac{\partial \tau_{yx}}{\partial x} + \dfrac{\partial \sigma_{yy}}{\partial y} + \dfrac{\partial \tau_{yz}}{\partial z} \\[2mm] \dfrac{\partial \tau_{zx}}{\partial x} + \dfrac{\partial \tau_{zy}}{\partial y} + \dfrac{\partial \sigma_{zz}}{\partial z} \end{bmatrix}
- \rho_{11}
\begin{bmatrix} \dfrac{\partial S}{\partial x} \\[2mm] \dfrac{\partial S}{\partial y} \\[2mm] \dfrac{\partial S}{\partial z} \end{bmatrix}
+ \left(\rho_{12} + \rho_{11}\right)
\begin{bmatrix} b_x\left(V_x - v_x\right) \\[2mm] b_y\left(V_y - v_y\right) \\[2mm] b_z\left(V_z - v_z\right) \end{bmatrix}, \quad (1)
$$

2) Velocity component of the solid phase

$$
\left(\rho_{11}\rho_{22} - \rho_{12}^2\right)
\begin{bmatrix} \dfrac{\partial v_x}{\partial t} \\[2mm] \dfrac{\partial v_y}{\partial t} \\[2mm] \dfrac{\partial v_z}{\partial t} \end{bmatrix}
= \rho_{22}
\begin{bmatrix} \dfrac{\partial \sigma_{xx}}{\partial x} + \dfrac{\partial \tau_{xy}}{\partial y} + \dfrac{\partial \tau_{xz}}{\partial z} \\[2mm] \dfrac{\partial \tau_{yx}}{\partial x} + \dfrac{\partial \sigma_{yy}}{\partial y} + \dfrac{\partial \tau_{yz}}{\partial z} \\[2mm] \dfrac{\partial \tau_{zx}}{\partial x} + \dfrac{\partial \tau_{zy}}{\partial y} + \dfrac{\partial \sigma_{zz}}{\partial z} \end{bmatrix}
- \rho_{12}
\begin{bmatrix} \dfrac{\partial S}{\partial x} \\[2mm] \dfrac{\partial S}{\partial y} \\[2mm] \dfrac{\partial S}{\partial z} \end{bmatrix}
+ \left(\rho_{12} + \rho_{22}\right)
\begin{bmatrix} b_x\left(V_x - v_x\right) \\[2mm] b_y\left(V_y - v_y\right) \\[2mm] b_z\left(V_z - v_z\right) \end{bmatrix}, \quad (2)
$$

3) Stress component of the fluid phase

$$
\frac{\partial S}{\partial t} = Q_1 \frac{\partial V_x}{\partial x} + Q_2 \frac{\partial V_y}{\partial y} + Q_3 \frac{\partial V_z}{\partial z} + R\varepsilon, \tag{3}
$$

and 4) stress component of the solid phase

$$
\begin{bmatrix}
\dfrac{\partial \sigma_{xx}}{\partial t} \\[2mm]
\dfrac{\partial \sigma_{yy}}{\partial t} \\[2mm]
\dfrac{\partial \sigma_{zz}}{\partial t} \\[2mm]
\dfrac{\partial \tau_{yz}}{\partial t} \\[2mm]
\dfrac{\partial \tau_{xz}}{\partial t} \\[2mm]
\dfrac{\partial \tau_{xy}}{\partial t}
\end{bmatrix}
= \boldsymbol{D}_{6\times6}
\begin{bmatrix}
\dfrac{\partial v_x}{\partial x} \\[2mm]
\dfrac{\partial v_y}{\partial y} \\[2mm]
\dfrac{\partial v_z}{\partial z} \\[2mm]
\dfrac{\partial v_y}{\partial z} + \dfrac{\partial v_z}{\partial y} \\[2mm]
\dfrac{\partial v_x}{\partial z} + \dfrac{\partial v_z}{\partial x} \\[2mm]
\dfrac{\partial v_x}{\partial y} + \dfrac{\partial v_y}{\partial x}
\end{bmatrix}
+
\begin{bmatrix}
Q_1\varepsilon \\
Q_2\varepsilon \\
Q_3\varepsilon \\
0 \\
0 \\
0
\end{bmatrix} . \quad (4)
$$

In the equations above mentioned, $\sigma_{ii}|_{i=x,y,z}$ is normal stress of the solid phase while τ_{yz}, τ_{xz} and τ_{xy} are shear stress of the solid phase; S is normal stress of the fluid phase; $v_i|_{i=x,y,z}$ is particle velocity of solid material in i direction while $V_i|_{i=x,y,z}$ is particle velocity of fluid material in i direction; ρ_{11} is density of the solid material, ρ_{22} is density of the fluid material, and ρ_{12} is coupling density parameter; Q is the coupling parameter relating to bulk variation between the solid phase and the fluid phase, and R represents the elastic parameter relating to the fluid phase; ε is the bulk strain of the fluid phase; $b_i|_{i=x,y,z}$ is dissipation coefficient which satisfies $b_x=b_y=b_z$ in isotropic two-phase media and $b_x=b_y$ in vertical transversely isotropic Biot media; $\boldsymbol{D}_{6\times6}$, which varies in different media, is elastic coefficient matrix of the solid phase. In homogeneously isotropic media,

$$
\boldsymbol{D}_{6\times6} =
\begin{pmatrix}
A+2N & A & A & 0 & 0 & 0 \\
A & A+2N & A & 0 & 0 & 0 \\
A & A & A+2N & 0 & 0 & 0 \\
0 & 0 & 0 & N & 0 & 0 \\
0 & 0 & 0 & 0 & N & 0 \\
0 & 0 & 0 & 0 & 0 & N
\end{pmatrix}
$$

with only two separate elastic parameters A and N, while in transversely isotropic media,

$$
\boldsymbol{D}_{6\times6} =
\begin{pmatrix}
d_{11} & d_{12} & d_{13} & 0 & 0 & 0 \\
d_{21} & d_{22} & d_{23} & 0 & 0 & 0 \\
d_{31} & d_{32} & d_{33} & 0 & 0 & 0 \\
0 & 0 & 0 & d_{44} & 0 & 0 \\
0 & 0 & 0 & 0 & d_{55} & 0 \\
0 & 0 & 0 & 0 & 0 & d_{66}
\end{pmatrix} ,
$$

where, $d_{11}=d_{22}=\lambda_{||}+2\mu_{||}$, $d_{12}=d_{21}=\lambda_{||}$, $d_{13}=d_{23}=d_{31}=d_{32}=\lambda_{\perp}$, $d_{33}=\lambda_{\perp}+2\mu_{\perp}$, $d_{44}=d_{55}=\upsilon$, $d_{66}=\mu_{||}$ with five separate elastic parameters $\lambda_{||}$, $\mu_{||}$, $\mu_{\perp}$ $\lambda_{\perp}$, and υ.

3 Convolutional Forsyte polynomial differentiator

The interpolating function of the Forsyte polynomial can be written as (Xie, 1981)

$$
\phi(x) = C_0 P_0(x) + \sum_{j=1}^{n} C_j P_j(x) \quad (5)
$$

which is a generalized orthogonal polynomial. In the above equation,

$$
\begin{aligned}
&P_0 = 1 \\
&P_1(x) = (x-\alpha_1)P_0(x) \\
&P_2(x) = (x-\alpha_2)P_1(x) - \beta_1 P_0(x) \\
&P_3(x) = (x-\alpha_3)P_2(x) - \beta_2 P_1(x) \\
&\qquad\vdots \\
&P_{j+1}(x) = (x-\alpha_{j+1})P_j(x) - \beta_j P_{j-1}(x)
\end{aligned}
$$

where

$$
\alpha_1 = \frac{1}{m}\sum_{i=1}^{m} x_i, \quad
\alpha_{j+1} = \frac{\displaystyle\sum_{i=1}^{m} x_i P_j^2(x_i)}{\displaystyle\sum_{i=1}^{m} P_j^2(x_i)},
$$

$$
\beta_j = \frac{\displaystyle\sum_{i=1}^{m} x_i P_j(x_i) P_{j-1}(x_i)}{\displaystyle\sum_{i=1}^{m} P_{j-1}^2(x_i)},
$$

$$
C_0 = \frac{\displaystyle\sum_{i=1}^{m} f(x_i) P_0(x_i)}{\displaystyle\sum_{i=1}^{m} P_0^2(x_i)}, \quad
C_j = \frac{\displaystyle\sum_{i=1}^{m} f(x_i) P_j(x_i)}{\displaystyle\sum_{i=1}^{m} P_j^2(x_i)},
$$

$f(x_i)$ represents the value of the interpolated function $f(x)$ at the point x_i. $P_0(x)$, $P_1(x)$, $P_2(x)$, $\cdots$, $P_{j+1}(x)$ in equation (5) are defined as Forsyte polynomial system.

Taking the first-order derivative of equation (5) with respect to x obtains

$$
\phi'(x) = \frac{\mathrm{d}\phi(x)}{\mathrm{d}x} = C_1 + \sum_{j=2}^{N} C_j P_j'(x). \quad (6)
$$

Then, Forsyte polynomial differentiator is written as

$$
\frac{\mathrm{d}}{\mathrm{d}x} = C_1 + \sum_{k=2}^{N} C_k P_k'(x) \quad (7)
$$

where

$$
C_k = \frac{\displaystyle\sum_{i=1}^{m} P_k(x_i)}{\displaystyle\sum_{i=1}^{m} P_k^2(x_i)}.
$$

Equation (7) can be discretized as

$$d_1(i\Delta x) = C_1 + \sum_{j=2}^{N} C_j P'_j(i\Delta x), \qquad (8)$$

where, i is the sampling index and Δx is the sampling interval along x direction. A Gaussian function presented as follow is used to truncate equation (8).

$$\hat{d}_1(i\Delta x) = \begin{cases} (-1)^i d_1(i\Delta x)\, w(i) & i = 1, 2, \cdots, m \\ -\hat{d}_1(j\Delta x) & i = -1, -2, \cdots, -m; \quad j = -i \end{cases},$$

$$\hat{d}_1(0\Delta x) = 0.$$

(10)

In practice, we need to choose appropriate length and coefficients of the convolutional differentiator so that both local information and global information of the wave field can be taken into account. We used a 7-point differentiator, a 9-point differentiator and an 11-point differentiator to compute the derivatives, respectively and we find that the precision of the 7-point differentiator is obviously lower than that of the 9-point differentiator, while the precision of the 11-point differentiator is almost the same as that of the 9-point differentiator but the amount of calculation is larger. So by analysis and comparison, we choose the 9-point convolutional differentiator, which has a appropriate length for the computation of the derivatives, to compute the wave propagation in two-phase media.

Figure 1 shows the amplitude variation with sampling points of 9-point convolutional differentiator. As shown in Figure 1, the amplitude attenuates quickly and the optimal coefficients are antisymmetrical. These attributes of the convolutional differentiator are very important for taking both local and global information of the wave field into consideration.

We chose Gaussian function $f(x)=\exp(-a^2 x^2)$ (Li and Li, 2008) as the test function to test the accuracy of the 9-point CFPD. Figure 2 shows the result of comparison of the derivative obtained by 9-point Forsyte orthogonal polynomial (CFPD) with the result from pseudo-spectral method. We can see that the derivative obtained by 9-point CFPD is more accurate than that from pseudo-spectral method, fitting the analytical result very well. So it is confirmed that the 9-point
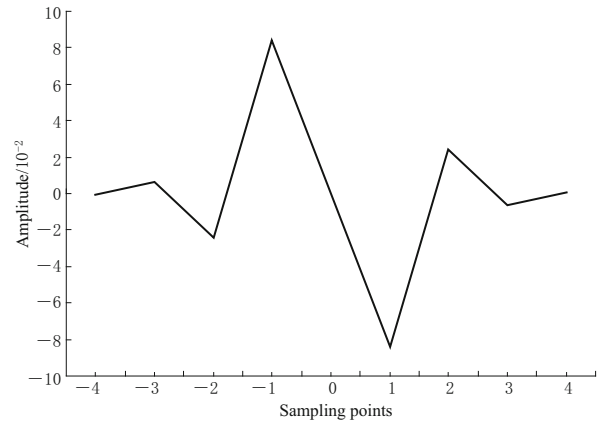
$$w(n) = ce^{-an\Delta x^2}, \quad |n| = 0,\ 1,\ 2,\ \cdots,\ mx. \qquad (9)$$

where, mx is the sampling number of unilateral truncated length, c is a constant and a ($0.1 \leq a \leq 0.75$) is the attenuation factor. By means of the window function (9), the first-order convolutional differentiator is derived.

Figure 1 Amplitude versus sampling points for 9-point convolutional differentiator.

CFPD can be used for the numerical modeling of seismic wave propagation.

In CFPD scheme introduced here, the spatial and temporal derivatives are obtained by CFPD method and staggered-grid finite difference method, separately.

By analysis, the stability condition of CFPD method can be written as $v\Delta t/\Delta d \leq \sqrt{2}/\pi$, which is similar to that of the pseudo-spectral method (Gazdag, 1981). In the above inequality, v is the maximal velocity of the media, Δt is the time sampling interval and Δd is the spatial sampling interval. This stability condition can effectively avoid the numerical dispersion caused by unreasonable parameters of the model in the process of computation.
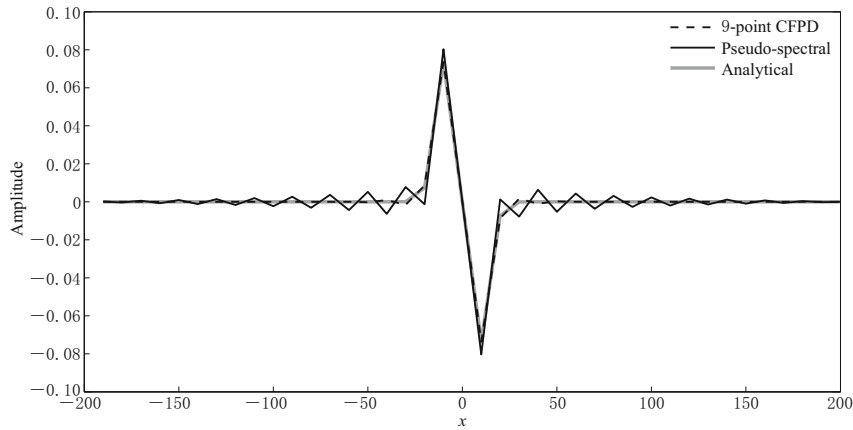
Figure 2   Comparison of accuracy of derivatives.

In order to absorb the artificial reflection from the computational edge, we adopt the PML absorbing boundary condition in Biot's equations to attenuate the outgoing waves and to eliminate the artificial reflections (Li, 2011).

4 Numerical experiments

In numerical modeling of seismic wave propagation, wavelet needs to be used to represent the source. Ricker wavelet and Gauss wavelet are two kinds of wavelets frequently used in numerical modeling. In this paper, we select Ricker wavelet as the source, of which the time function is

$$f(t) = [1 - (\pi f_0 t)^2] \exp[-(\pi f_0 t)^2]$$

and the space function is

$$f(x, z) = \exp\{-\alpha^2[(x - x_0)^2 + (z - z_0)^2]\}$$

where f_0 is the dominant frequency, (x_0, z_0) is the location of the source and α is a constant which controls the decay rate of the source impulse in space.

4.1   A homogeneously isotropic model

For a homogeneous 2D two-phase model, the parameters are listed in Table 1. The grid size is 256×256 with grid spacing $\Delta x = \Delta z = 10$ m and the time step is set as $\Delta t = 1$ ms. A Ricker wavelet with the dominant frequency of 25 Hz is used here as the seismic source, which is located at the coordinate (125, 125).

Table 1   Physical parameters of a homogeneous two-phase medium (from Pei, 2006)

Solid phase				Fluid phase		Coupling parameter		Dissipation coefficient b
d_{11}	d_{13}	d_{55}	ρ_{11}	R	ρ_{22}	Q	ρ_{12}	
26.4	12.72	6.84	2.17	0.331	0.191	0.953	−0.083	3.00

Note: d_{ij}, R and Q are in unit of 10^9 kg·m^{-1}·s^{-2}, b is in unit of kg·m^{-3}·s^{-1} and ρ_{ij} is in 10^3 kg·m^{-3}.

Figures 3 and 4 clearly show that three kinds of waves, fast P-wave P^1, S-wave S and slow P-wave P^2, exist in the wave field propagating in homogeneously isotropic two-phase media. The slow P-wave P^2, which is able to indicate the existence of oil/gas or water, is a special wave existing in two-phase media (Meng et al., 2003). Seismic waves in the solid phase and fluid phase are coupled with each other. Fast P-waves in the solid phase and fluid phase are in phase with each other while slow P-waves are out of phase with each other, as seen in Figure 4. Moreover, the amplitude of slow P-wave in the fluid phase is much larger than that in the solid phase. Additionally, we can see that P^2's am-

plitude is even larger than S's in the fluid phase at this time (t=280 ms), this perhaps because that the dissipation coefficient b is so small here that the attenuation of slow P-wave is not quick. In fact, slow P-wave attenuates very quickly in the Earth and its amplitude is affected by the parameter b (Biot, 1956a, b; Zhang et al., 2008). Generally, the true values of b in the Earth are fairly large, leading to very quick attenuation of the amplitude of slow P-wave and that is the reason why we cannot always observe the slow P-wave in seismic explorations. The fast P-wave is what we use in seismic explorations.
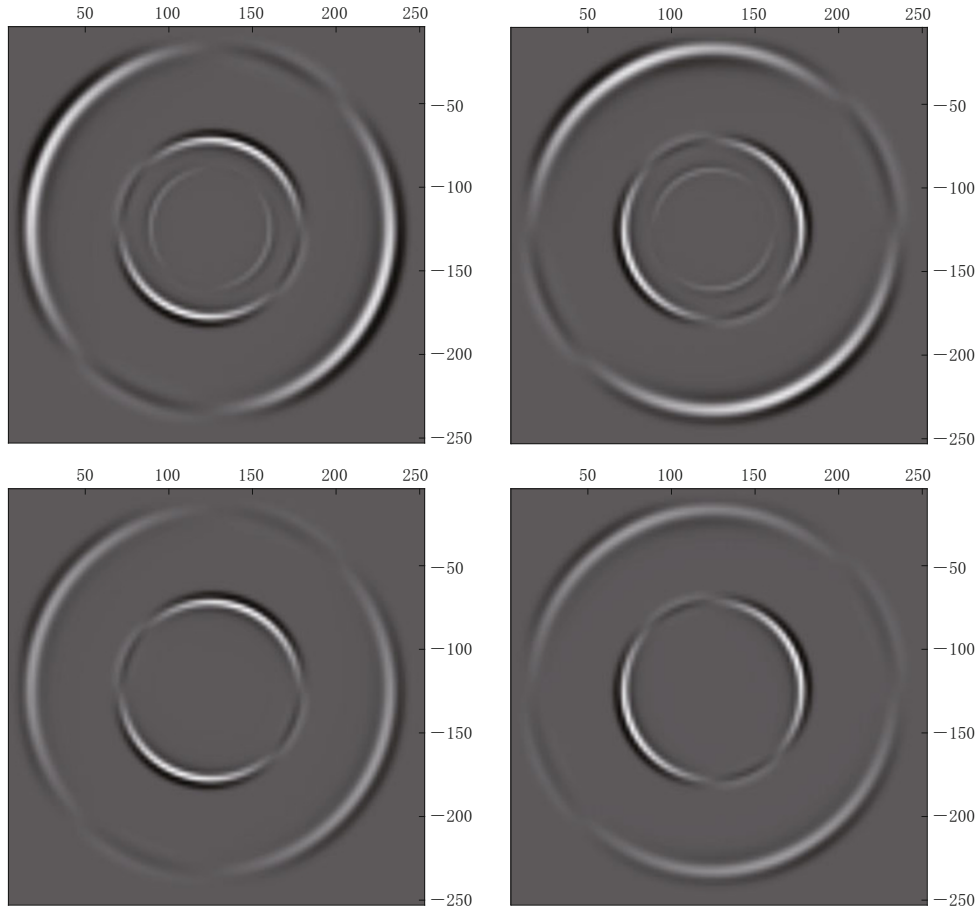
Figure 3   Snapshots of the x components (left) and the z components (right) at t=400 ms for 2D isotropic two-phase media. Top two panels are for fluid phase, and bottom panels for solid phase.
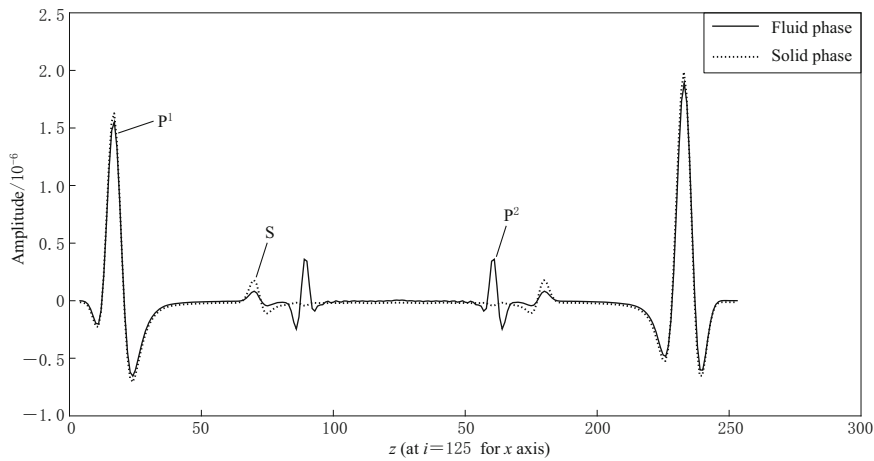

Figure 4   Seismograms of vertical component of the fluid phase (solid line) and the solid phase (dashed line) at one point (i=125) along a vertical line.

4.2   Anisotropic models
4.2.1   Transversely isotropic two-phase media

For wave propagation in the anisotropic two-phase media, the elements of the elastic coefficient matrix $\boldsymbol{D}_{6\times6}$ need to satisfy the conditions of conservation of energy:

$$d_{11} \geq 0, d_{33} \geq 0, d_{55} \geq 0, E^2 = d_{33}d_{11} - d_{13}^2 \geq 0$$

where, d_{13} and d_{55} are two key elements that affect the velocity of wave propagation and the shapes of wavefronts in transversely isotropic media (He and Zhang, 1996). Therefore, next we will take transversely isotropic two-phase media as an example to investigate the characteristics of wave propagation in anisotropic media.

To examine the effects of coefficients d_{13} and d_{55} on wave propagation, we make a scheme as follow: firstly, change the value of d_{13} and keep d_{11}, d_{33} and d_{55} to be constant; secondly, change the value of d_{55} and keep d_{11}, d_{33} and d_{13} to be constant. The grid size is 200×200 with grid spacing 10 m and the time step is 1 ms. The seismic source is a Ricker wavelet with the dominant frequency of 15 Hz and the location is at (100, 100). The parameters are listed in Table 2. The transversely isotropic two-phase media used here are zero-azimuth with z being the principal axis of symmetry. Figure 5 shows the snapshots of waves.

Table 2   Physical parameters of transversely isotropic two-phase media

No. in Fig.5	Solid phase						Fluid phase		Coupling parameters			Dissipation coefficient	
	d_{11}	d_{13}	d_{33}	d_{55}	d_{66}	ρ_{11}	R	ρ_{22}	Q_1	Q_3	ρ_{12}	b_{11}	b_{33}
a	26.4	−10	15.6	4.38	6.84	2.17	0.331	0.191	1.14	0.953	−0.083	0.5	3
b	26.4	1	15.6	4.38	6.84	2.17	0.331	0.191	1.14	0.953	−0.083	0.5	3
c	26.4	9	15.6	4.38	6.84	2.17	0.331	0.191	1.14	0.953	−0.083	0.5	3
d	26.4	12.72	15.6	4.38	6.84	2.17	0.331	0.191	1.14	0.953	−0.083	0.5	3
e	26.4	12.72	15.6	20	6.84	2.17	0.331	0.191	1.14	0.953	−0.083	0.5	3
f	26.4	12.72	15.6	27	6.84	2.17	0.331	0.191	1.14	0.953	−0.083	0.5	3

Note: d_{ij}, R and Q are in unit of 10^9 kg·m^{-1}·s^{-2}, b is in unit of kg·m^{-3}·s^{-1} and ρ_{jj} is in 10^3 kg·m^{-3}.

A lot of information can be obtained by observing Figure 5. First of all, fast P-wave P^1, S-wave S and slow P-wave P^2 as denoted by A, B and C respectively, are clearly seen in Figure 5c. The wavefronts are elliptic instead of circular because the velocities of the seismic waves are different along different directions. Secondly, the wavefronts of S-wave become sharp-angled and intersected, as clearly shown in Figure 5b. We see that S-wave splitting, which is caused by the anisotropy of the media, occurs in many directions except the intersection directions. S-wave splits into two kinds of waves: the fast S-wave S^1 and the slow S-wave S^2, as marked in Figure 5b. But in the directions of the intersection the two kinds of S-waves have the same propagation speed causing no splitting (Liu and Li, 2000; Pei, 2006). In addition, d_{13} and d_{55} have important influence on the shapes of wave field. When d_{55} is constant, the intersections diminish and vanish finally with d_{13} increasing (Figure 5a–5d) and when d_{13} is constant, the intersections reappear with d_{55} increasing (Figure 5d–5f). Meanwhile, the wavefront of P^1 transforms from a rhombus to an ellipse and then to a square. By analysis on the anisotropic characteristics of wave propagation mentioned above, we could infer crack orientations and reservoir structure so that we can know where oil and gas exist. The strong anisotropic characteristics and dispersion of the fast and slow P-waves depend on permeability anisotropy, which is related to the crack orientations. Therefore, the attenuation and dispersion characteristics of fast and slow P-waves as well as S-wave splitting are the important factors indicating crack orientations and reservoir structure (Yang et al., 2000).

4.2.2   A layered fault model

Now we present a layered fault model of isotropic two-phase media to detect the effects from the interface and the fault. A 30 m high fault of which the top interface is located at $z=100$ m and the bottom interface is located at $z=130$ m, is set in the model (Figure 6). The physical parameters of the media are shown in Table 3 below. The grid used here and the time step are the same as the ones in the transversely isotropic model. The seismic source is set as a 20 Hz Ricker wavelet located at (100, 80) and the wavefield is seen in Figure 7.

As shown in Figure 7, the wavefield affected by the fault is very complicated. Not only the transmitted, reflected and refracted waves caused by the interface but the diffracted waves generated by the fault step are also clearly presented in the snapshots. We can see the conversions between the three types of waves (fast P-waves, S-waves and slow P-waves) on the interface and the fault. Additionally, we can also find that few frequency dispersions occur in the wave field. Referring to the outcome obtained by Dai et al. (1995) using finite

difference method and the outcome obtained by Zhang et al. (2008) using pseudo-spectral method, we can confirm that this convolutional differentiator method is ap-

plicable for the wave field modeling in heterogeneously layered media, which is of great significance to the seismic exploration.
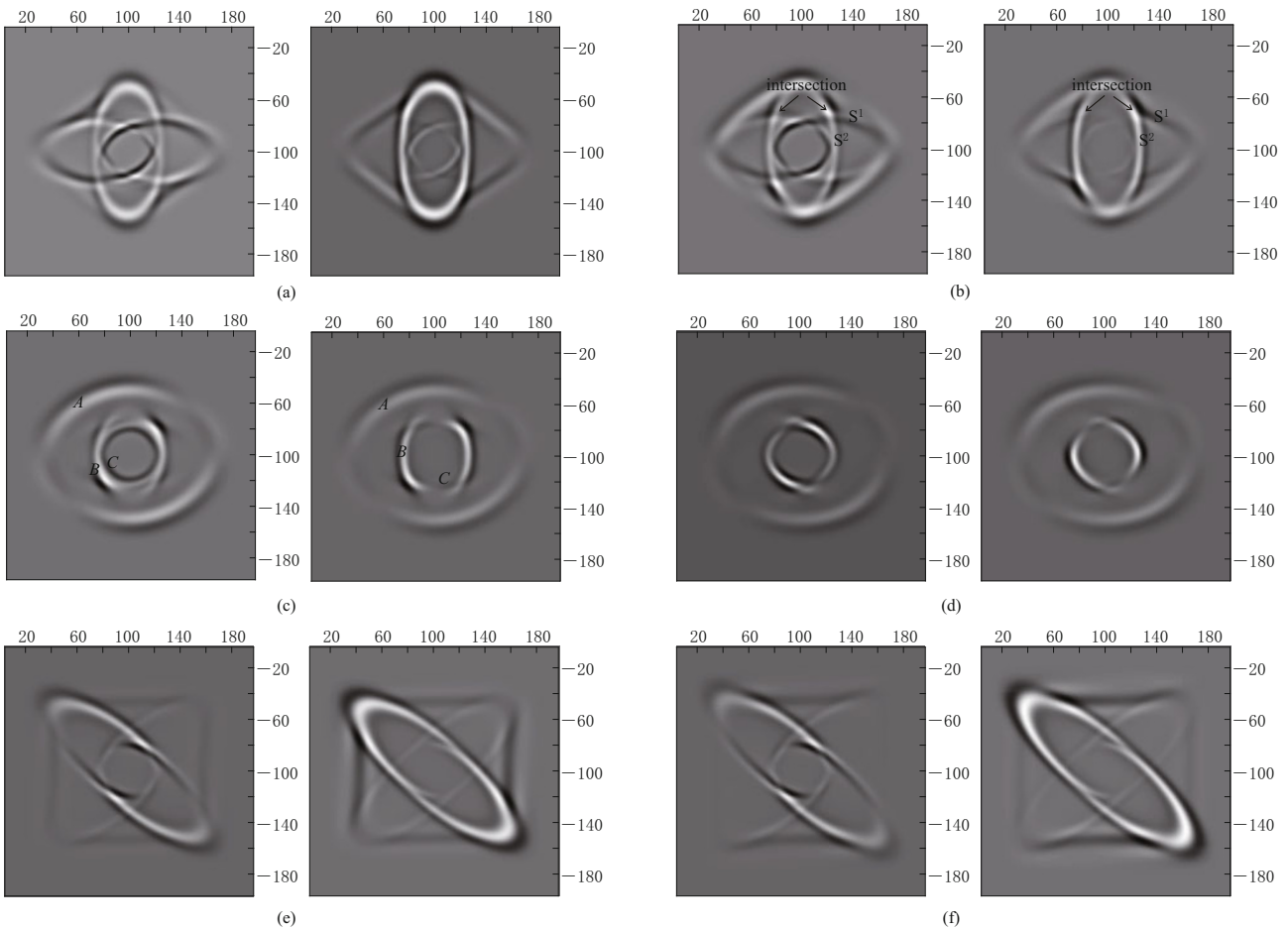

Figure 5   Snapshots of the vertical components of fluid phase (left in subfigure a–f) and solid phase (right in subfigure a–f) at t=280 ms for 2D transversely isotropic two-phase media with varying d_{13} and d_{55} from (a) to (f) corresponding to (a) to (f) in Table 2. In Figure 5c, A, B, and C denote the fast P-wave, S-wave and slow P-wave. S-wave splitting can be clearly observed in the figure, leading to the intersections of the wavefronts of S-wave, as marked in Figure 5b.
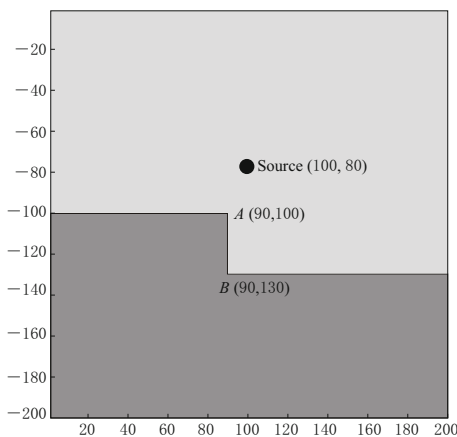

Figure 6   A layered fault model.

5 Discussion and conclusions

Based on generalized Forsyte orthogonal polynomial, the characteristics of waves in two-phase media have been studied by using a convolutional differentiator method. Meanwhile, we used the staggered-grid finite difference scheme to calculate the temporal derivative of the first-order velocity-stress wave equation of two-phase media. The results from a homogeneously isotropic model and a transversely isotropic model confirm the conclusions derived by Biot's theory. The interface effects can also be well modeled using the CFPD method.

The accuracy test comparing this method with pseudo-spectral method shows that this method has high accuracy. The local and global information can be
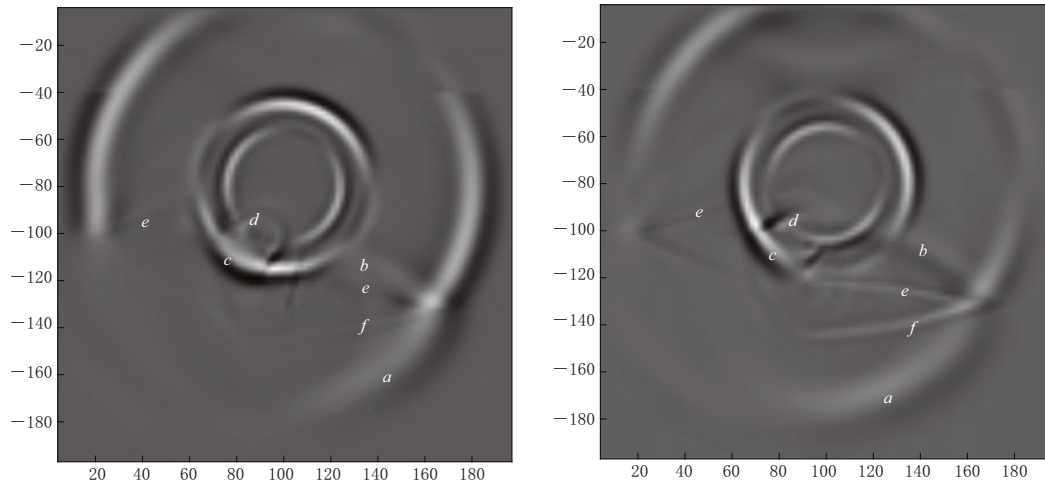
Figure 7   Snapshots of the horizontal component (left) and vertical component (right) at $t=300$ ms for the layered fault model (fluid phase). Waves generated by the interface, i.e., a and b denote the transmitted P-wave and reflected P-wave, c is trasmitted SV-P wave, d is diffracted wave generated by the fault step, and e and f are refracted waves. The slow P-wave can be clearly seen in the top layer but no transmitted slow P-waves are observed in the bottom layer because of the high value of dissipation coefficient b. The slow P-wave is converted to fast P-wave (P^2–P^1) diffracted out from the fault edge when hitting the fault step.

Table 3   Physical parameters of a two-layer model (from Dai et al., 1995)

Solid phase				Fluid phase		Coupling parameters		Dissipation coefficient
d_{11}	d_{13}	d_{55}	ρ_{11}	R	ρ_{22}	Q	ρ_{12}	b
34.0	20.33	6.84	2.167	0.331	0.191	0.953	−0.083	3.00
79.7	55.65	12.0	2.43	0.790	0.255	0.700	−0.100	7000

Note: The parameters are in the same units as those in Table 2.

considered at the same time by optimizing the coefficients of the operator and adjusting the operator length. As it has been investigated, both local and global information of the wave field has been considered so that fine resolution of the anisotropic media is obtained.

This research can be easily extended to the deep process accompanied by fluid beneath active orogen belt. The deep medium and tectonic environment of the earthquake "pregnancy", generation and development are very complicated with the characters of heterogeneity and anisotropy. As we all know, the seismic source media are broken undergoing the force process. Consequently, the structure of the media is changed as well as the deep fluid moving and upwelling along the fault and weak belt. Therefore it is necessary to develop the theory of two-phase media for further research on the seismic wave kinetics in deep environment (Teng et al., 2009). Additionally, the theory for two-phase media will be of great significance in the applications of deep oil and gas prospecting.

References

Biot M A (1956a). Theory of propagation of elastic waves in a fluid-saturated porous solid. I. Low-frequency range. *J Acoust Soc Am* **28**: 168–178.

Biot M A (1956b). Theory of propagation of elastic waves in a fluid-saturated porous solid. II. Higher frequency range. *J Acoust Soc Am* **28**: 179–191.

Cheng B J, Li X F and Long G H (2008). Seismic waves modeling by convolutional Forsyte polynomial differentiator method. *Chinese J Geophys* **51**(2): 531–537 (in Chinese with English abstract).

Dai N, Vafidis A and Kanasewieh E R (1995). Wave propagation in heterogeneous, porous media: A velocity-stress,

finite difference method. *Geophysics* **60**(2): 327–340.

Gassmann F (1951). Elastic waves through a packing of spheres. *Geophysics* **16**(4): 673–685.

Gazdag J (1981). Modeling of the acoustic wave equation with transform methods. *Geophysics* **46**: 854–859.

He Q D and Zhang Z J (1996). *Seismic Wave in the Transversely Isotropic Media and the Numerical Modeling.* Jilin University Press, Changchun (in Chinese).

Li X F (2011). PML absorbing boundary condition for seismic numerical modeling by convolutional differentiator in fluid-saturated porous media. *Journal of Earth Science* **22**(3): 377–385.

Li X F and Li X F (2008). Numerical simulation of seismic wave propagation using convolutional differentiator. *Earth Science — Journal of China University of Geosciences* **33**(6): 861–866 (in Chinese with English abstract).

Liu Y and Li C C (2000). Study of elastic wave propagation in two phase anisotropic media by numerical modeling of pseudospectral method. *Acta Seismologica Sinica* **13**(2): 143–150.

Liu Y and Wei X C (2003). Finite element equations and numerical simulation of elastic wave propagation in two-phase anisotropic media. *Acta Seismologica Sinica* **16**(2): 166–174.

Meng Q S, He Q D, Zhu J W and Wang D L (2003). Seismic modeling in isotropic porous media based on BISQ model. *Journal of Jilin University* (*Earth Science Edition*) **33**(2): 217–221 (in Chinese with English abstract).

Niu B H, Wu Y X and Sun C Y (1994). The numerical modeling anisotropic medium containing fluid filled cracks and dry cnacks. *Journal of Changchun University of Science and Technology* **24**(4): 454–460 (in Chinese with English abstract).

Pei Z L (2006). A staggered-grid high-order finite difference method for modeling elastic wave equation in 3-D dual-phase anisotropic media. *Journal of China University of*

Petroleum (*Edition of Natural Science*) **30**(2): 16–20 (in Chinese with English abstract).

Shao X M and Lan Z L (2000). Finite element methods for the equations of waves in fluid-saturated porous media. *Chinese J Geophys* **43**(2): 264–278 (in Chinese with English abstract).

Sun W T and Yang H Z (2004). Elastic wave field simulation with finite difference method in two-phase anisotropic medium. *Acta Mechanica Solida Sinica* **25**(1): 21–28 (in Chinese with English abstract).

Teng J W, Zhang Z J, Yang D H, Zhang Y Q, Zhang X M, Yang H and Ruan X M (2009). The seismic wave propagation theory and the deep medium and tectonic environment of the earthquake "pregnancy", generation and development. *Progress in Geophysics* **24**(1): 1–19 (in Chinese with English abstract).

Xie J (1981). *Mathematical Methods for the Data Processing of Geophysical Prospecting.* Geological Publishing Press, Beijing, 97–104 (in Chinese).

Yang D H (2002). Finite element method of the elastic wave equation and wavefield simulation in two-phase anisotropic media. *Chinese J Geophys* **45**(4): 575–583 (in Chinese with English abstract).

Yang D H, Zhang Z J, Teng J W and Wang G J (2000). The study of two-phase anisotropy questions and applied prospects. *Progress in Geophysics* **15**(2): 7–21 (in Chinese with English abstract).

Zhu X and McMechan G A (1991). Numerical simulation of seismic responses of poroelastic reservoirs using Biot theory. *Geophysics* **56**(3): 328–339.

Zhou B and Greenhalgh S A (1992). Seismic scalar wave equation modeling by a convolutional differentiator. *Bull Seismol Soc Am* **82**(1): 289–303.

Zhang J D, Le Y X and Wang Y X (2008). Numerical modeling of seismic wave field in isotropic porous media using pseudo-spectral method. *Geophysical Prospecting for Petroleum* **47**(4): 338–345 (in Chinese).